

Self-supervised Exposure Trajectory Recovery for Dynamic Blur Estimation

Youjian Zhang[†], Chaoyue Wang[†], Stephen J. Maybank[‡], Dacheng Tao[†]

[†]UBTECH Sydney AI Centre, Faculty of Engineering, The University of Sydney

[‡] Department of Computer Science and Information Systems, Birkbeck College

Abstract

Dynamic scene blurring is an important yet challenging topic. Camera sensors record both latent sharp content and complex motions (*e.g.*, camera shake and object motion and deformation) during exposure of a dynamic scene. A dynamic blurry image represents an accumulated exposure result over a period of time. Benefiting from their powerful fitting capacity, deep learning-based methods have achieved impressive performance for dynamic scene deblurring. However, the time-dependent motion information contained in a blurry image has yet to be fully explored and accurately formulated because: (i) the ground truth of blurry motion is difficult to obtain and represent; (ii) the temporal ordering of blurry motion is destroyed during the accumulation process; and (iii) similar to blur removal, dynamic motion estimation is highly ill-posed. By revisiting the principle of camera exposure, dynamic blur can be described by the relative motions of sharp content with respect to each exposed pixel. This understanding motivates us to define exposure trajectories, which record the trajectories of relative motions during an exposure period to represent the motion information contained in a blurry image and explain the causes of dynamic blur. We propose a new blur representation, which we call *motion offset*, to model pixel-wise displacements of the latent sharp image at multiple timepoints. Under mild assumptions/constraints, the learned motion offsets can recover dense, (non-)linear exposure trajectories, which significantly reduce temporal disorder and ill-posed problems. Finally, we demonstrate that the estimated exposure trajectories can fit real-world dynamic blurs and further contribute to motion-aware image deblurring and warping-based video extraction from a single blurry image. Comprehensive experiments on benchmarks and challenging real-world cases demonstrate the superiority of the proposed framework over state-of-the-art methods. More video results can be found in our supplementary video.

1 Introduction

Dynamic scene blurring caused by camera shake, object motion, or depth variation is one of the commonest image degradations. Estimating motion information and restoring sharp contents in dynamic blurry images would benefit many real-world applications including segmentation, detection, and recognition. Benefiting from the powerful fitting ability of deep convolutional neural networks (CNNs), deep learning-based deblurring methods [23, 9, 51, 30] have achieved impressive performance for dynamic blur removal. Nevertheless, exploring dynamic information in blurry images remains an academic and commercial challenge.

Most conventional blur removal methods are based on blur kernel estimation [8, 15, 42, 21, 13, 14, 29], which assumes that a blurry area can be represented as a weighted sum of its latent sharp surrounding content. A blur kernel is actually a weighted matrix that performs convolution on a sharp image patch to synthesize a blurry pixel. Conversely, blur kernel estimation is cast as an energy minimization problem which aims to recover both the blur kernels and the latent sharp image from a blurry image. Such optimizations are highly ill-posed, so most conventional methods are restricted by assumptions of motion types and predefined image priors. For example, [42, 12, 46, 54] only handle blur caused by camera rotations, in-plane translations, or forward out-of-plane translations. For more complex dynamic blur, identifying a suitably informative and general prior is extremely difficult.

Accompanying the development of deep neural networks, learning-based methods [11, 41] have been proposed to estimate blur kernels directly from blurry images. Compared to optimization-based methods, learning-based methods utilize predefined kernels to synthesize blurry data and then train an estimation network in a supervised manner. A well-trained estimation network is usually more effective and efficient at modeling object motion blur. However, due to the inherent limitations of blurry data synthesis, existing predefined blur kernels only cover limited motion types such as 2D vectors (*i.e.*, linear motions), as in [11]. As a consequence, these methods may not be as effective for complex real-world dynamic scene blur.

Taking advantage of advanced photographic equipment, dynamic scene datasets [23, 39] containing high frame-rate videos have been compiled to further understand dynamic blur. A real-world blurry image can be regarded as an accumulation of multiple “instant” frames, where a sequence of instant frames implicitly records blur (motion) information during an exposure period. Some methods [16, 31] are trained to directly recover these high frame-rate sharp frames without explicitly depicting dynamic motions. Moreover, in some video deblurring studies [4, 22], optical flow is estimated between adjacent frames as another motion representation. However, since optical flow between two frames is inherently linear and multiple frames may be misaligned, the estimated optical flow cannot perfectly match the dynamic motion contained in a single blurry image.

Therefore, significant efforts have been made to understand and estimate dynamic blur to benefit deblurring [11, 40], video extraction [31, 16], and 3D scene reconstruction [32]. However, time-dependent motion information contained in a dynamic blurry image has yet to be fully explored and accurately formulated, with existing blur representations (*e.g.*, blur kernels, motion flow, and optical flow) limited by synthetic ground truths, predefined priors, or temporal disorder. Here we aim to deliver more accurate blur estimation from a single blurry image. According to camera exposure principles, dynamic blur is caused by the relative motions of sharp content with respect to each exposed pixel. Inspired by this principle, we define the trajectories of these relative motions as exposure trajectories and demonstrate that learning exposure trajectories potentially has the following advantages. First, an exposure trajectory can clearly represent and directly visualize the relative motions that caused a blur. Second, compared to geometry-based blur kernels, an exposure trajectory takes account of temporal (ordering) information. Across equal time intervals, a relatively long trajectory reflects a higher relative velocity. Third, in contrast to the estimated piecewise linear optical flow, an exposure trajectory is continuous and is therefore unaffected by misalignment.

To recover the exposure trajectories of a dynamic blurry image, we propose a new blur representation, which we call *motion offset*. In contrast to existing blur representations, motion offsets model pixel-wise displacements of the latent sharp image at different timepoints. By simulating a camera exposure process, a set of motion offsets can be applied to a sharp image to synthesize a blurry output. To overcome the ill-posed nature of blur estimation (*i.e.*, potentially different motion solutions), we further apply a variety of constraints to ensure that the learned motion offsets form different types of trajectories, *e.g.*, linear, bi-directional linear, or even quadratic curves. Note that the proposed motion offsets and related constraints can easily be added into deep neural networks for backpropagation with other components. In this way, a self-supervised reblurring cycle can be performed to recover motion offsets (*i.e.*, exposure trajectories) of a blurry image. Compared to current learning-based methods, our model is trained on blurry/sharp image pairs and does not require any dynamic motion ground truths.

We successfully apply the learned exposure trajectories to related applications. For image deblurring, we devise a motion-aware deblurring module that takes pixel-wise trajectories to modulate the shape of convolution filters. Experiments show that the proposed motion-aware module enables a more effective deconvolution operation to handle large-scale dynamic blur with excellent results. In addition, warping-based video extraction from a single blurry image can easily be achieved using the learned exposure trajectories. Compared to existing video extraction models, our solution does not require any motion (or video) ground truths and is capable of interpolating an arbitrary number of middle frames, *i.e.*, derives slow-motion videos.

In summary, the contributions of this work are four-fold:

- We propose a novel representation, which we term motion offsets, to model the causes of dynamic blur. In contrast to conventional blur kernels, our motion offsets represent pixel-wise spatial displacements over a time sequence. Since they are dense, compact, and differentiable, the proposed motion offsets

are easily integrated into deep networks. A self-supervised training scheme is then devised for dynamic motion estimation from a single blurry image.

- To address the ill-posed nature of dynamic blur estimation, we propose multiple constraints on the motion offsets such that the learned trajectories follow certain patterns. Specifically, we implement linear, bi-directional linear, and quadratic constraints, and in doing so demonstrate that our motion offsets with non-linear quadratic constraints outperform existing methods for fitting realistic dynamic blur.
- With the learned exposure trajectories, we apply them to image deblurring and video extraction. We demonstrate the effectiveness of utilizing motion offsets to construct a motion-aware and compact deblurring module. We also provide a solution to video extraction, which is able to generate arbitrary numbers of intermediate frames from a blurry image.
- We present extensive analysis and evaluations on both synthetic datasets and dynamic scene deblurring benchmarks to demonstrate the superiority of our exposure trajectory recovery scheme over state-of-the-art methods.

2 Related Work

Single image blur estimation and removal have been extensively studied, with many methods proposed to solve different deblurring or blur estimation problems. Here, we focus our discussion on recent motion/dynamic blur studies, reviewing optimization- and learning-based methods for blur estimation and removal, respectively.

2.1 Optimization-based Methods

A blur process is conventionally modeled as a convolution operation in which blur kernels are applied to a latent sharp image to generate a blurry output. Given a blurry image, optimization-based methods aim to iteratively recover its deblurred result and the blur kernels that model blur motions. However, this problem is ill-posed, so optimization-based methods adopt predefined image priors [8, 15, 5, 36, 6, 47, 27, 28] or specific camera motion types [25, 12, 46, 54] to constrain the solution space of the blur kernels. For example, Tai *et al.* [42] proposed a general projective motion model for cameras undergoing ego motion. Gupta *et al.* [12] generalized camera motion to 2D translation and in-plane rotation and modeled them as motion density functions. Whyte *et al.* [46, 45] focused on solving the non-uniform blur caused by camera shake, aiming to recover the 3D rotation of the camera during an exposure process. Zheng *et al.* [54] attempted to handle another type of motion blur in which the camera moves primarily forwards or backwards by exploring homographies associated with different 3D planes. Overall, under predefined priors/assumptions, the ill-posed optimization problem becomes solvable, and these methods have achieved reasonable performance on specific blurry data. However, most of these priors assume that the underlying scene is static and that the blur is caused by camera motion rather than the movement of objects in the captured image.

However, it is difficult to identify a suitably informative and general prior for object motion within a dynamic scene. Therefore, some authors [26, 38, 13] have segmented different types of motion blur to overcome this problem. For example, Hyun *et al.* [13] proposed a novel energy function designed from the weighted sum of multiple blur data models. To handle different types of motion, their method estimated different motion blurs and their associated pixel-wise weights. Then, [26] proposed soft-segmentation for object layer estimation. By jointly estimating object segmentation and camera motion, they achieved favorable object motion blur removal performance. Although motion segmentation seems an ideal extension of optimization-based methods, it is hard to estimate an accurate segmentation due to ambiguous pixels between regions. Furthermore, even within a segmented area, existing priors can only handle a limited number of motion types.

2.2 Learning-based Methods

In order to overcome the limitations of manually designed image priors or specific camera motions, learning-based methods aim to directly predict blur kernels (or deblurred results) from an input blurry image. Benefiting from the development of CNNs, learning-based models can be trained on a large amount of blurry data and can perform blur estimation (or removal) in an end-to-end manner.

Most learning-based methods were originally proposed to estimate blur causes/representations from blurry images [25, 17, 1, 35]. For example, [1, 17] attempted to identify the type of blur from a restricted set of parametrized blurs. Schuler *et al.* [35] proposed a CNN module for learning a gradient-like representation and estimated the blur kernels by dividing the learned representation in Fourier space. Similarly, [3] predicted the Fourier coefficients of a deconvolution kernel that modeled blind motions of an image patch. Sun *et al.* [41] proposed a CNN-based model to predict the probabilistic distribution of motion blur at the patch level. In their method, a well-trained model estimated the direction and length of non-uniform linear motions. Then, [11] developed a fully convolutional framework to achieve pixel-wise prediction of blur kernels. Compared to optimization-based methods, these learning-based methods were more flexible and more efficiently estimated motion/dynamic blur. However, during training, most learning-based methods required the ground truths of blur representations for supervision. Since the ground truths of real-world blurry data are rarely available, these methods were trained on artificially-generated training examples, limiting the approach to some simple blur types (*e.g.*, linear motion). For more complex real-world dynamic motion, new blur representations and learning schemes are required to improve the estimations.

Accompanying the increased fitting capability of CNNs, many learning-based methods have been proposed to directly restore the latent sharp image from a blurry input [23, 43, 9, 19, 52, 24, 51, 44]. Among these methods, [23] proposed a multi-scale network which performed deblurring in a “coarse-to-fine” pipeline. Then, [43, 9] further improved on this strategy by altering the parameter sharing and independent scheme. By combining three CNNs and a recurrent neural network (RNN), Zhang *et al.* [52] employed the learned variant RNN weights to model spatial-variant blurs. Inspired by [52], many methods [40, 30, 50] have adopted a spatial-variant convolutional module as a substitute for some of the original convolution layers to increase the size of the receptive field in a more compact way. In addition, Kupyn *et al.* [19] and Ramakrishnan *et al.* [33] combined deblurring with generative adversarial networks (GANs) to synthesize more realistic sharp images. Overall, the combination of recently established real-world blurry datasets [23] and the powerful learning capability of CNNs have allowed learning-based methods to achieve impressive performance for directly synthesizing deblurred images. Unfortunately, the causes of blur (motions) are generally ignored in these works, preventing the exploration of the rich dynamic information contained in blurry images and introducing training difficulties for related tasks due to a poor understanding of dynamic blur. For example, in the absence of motion information, some deblurring and video extraction approaches either require a large receptive field to model large-scale dynamic blur [52] or require a complex training scheme and iterative inferences [16, 31]. In this work, we show that improving blur estimation can contribute to overcoming these problems and solving these tasks.

3 Motion Exposure Mechanism

When a camera takes a photograph, the exposure time cannot be instant due to technological constraints and physics (*i.e.*, exposure requirements). Therefore, a photograph records a target scene over a period of time. The exposure process can be formulated as:

$$B = \int_0^\tau H(L, t) dt, \quad (1)$$

where L represents the latent content/scene in the photograph, $H(L, t)$ denotes the instant frame at time t , and τ denotes the camera exposure time. Due to camera shake or the motion or deformation of objects in the scene, $H(L, t)$ may continuously vary with respect to time, leading to dynamic scene blurry image B .

In this work, we assume the middle instant sharp frame L_s records all visual information of latent content/scene L .¹ According to the principle of camera exposure, the function $H(L_s, t)$ can be defined as an image wrapping operation that performs a pixel-wise shift over different times, *i.e.*,

$$H(L_s, t) = L_s(\mathbf{P} + \Delta\mathbf{P}^t), \quad (2)$$

where \mathbf{P} denotes all pixels in L_s , and $\Delta p^t = (\Delta x^t, \Delta y^t)$ is the shift of pixel (x, y) at time t . In general, Eq. (1) and (2) represent the physical process of camera exposure. If a dynamic scene is recorded, this system of equations describes the motion exposure mechanism.

Assuming the brightness remains constant during exposure, we consider Eq. (1) and (2) and discretize them over multiple time steps N to derive the formation of a blurry pixel p_0 as:

$$B(p_0) = \frac{1}{N} \sum_{n=0}^{N-1} L_s(p_0 + \Delta p_0^{t_n}), \quad (3)$$

which means a blurry pixel can be represented as the accumulation of pixels in the latent sharp image moved by Δp^{t_n} . In this work, instead of deriving the blur kernels of a blurry image, we directly focus on the spatial shift Δp^{t_n} of each pixel. Thus, we propose a new time-dependent blur representation, *motion offset*. Similar to conventional blur kernels, the proposed motion offsets directly act on sharp images and then output blurry results. In contrast, our motion offsets model the blur formation as a spatial shift through time.

3.1 Blur Creation Module

Based on the proposed motion offset and motion exposure mechanism, we devise a *blur creation module* which takes one sharp image L_s and motion offsets $(\{\Delta\mathbf{P}^{t_n}\}_{t_n=1}^N)$ as inputs to generate a dynamic blurry image. For each blurry pixel (*i.e.*, exposure location) p , the proposed *blur creation module* is asked to locate pixels $p^{t_n} = p + \Delta p^{t_n}$ in a latent sharp image L_s (Eq. (3)) and further average them to obtain a blurry pixel. Since a real-world dynamic motion is continuous, we employ the bilinear interpolation to calculate the pixel value of location p^{t_n} ,

$$L_s(p + \Delta p^{t_n}) = L_s(p^{t_n}) = \sum_q G(q, p^{t_n}) \cdot L_s(q), \quad (4)$$

where q enumerates the referenced neighborhood points of the sampling location p^{t_n} , and $G(\cdot, \cdot)$ is the bilinear interpolation kernel. As illustrated in Fig. 1, our motion offsets are of the same spatial resolution as the input image. Each offset has two channels corresponding to 2D axes. In practice, the *blur creation module* takes N motion offsets and a sharp image L_s as inputs and synthesizes an averaged blurry output.

3.2 Discussion

Compared to conventional blur kernels, the proposed motion offsets aim to mimic the exposure process of a camera sensor. If we assume the latent content/scene is known, motion offsets encode motion/dynamic information during an exposure period and can further synthesize a blurry image. Mathematically, the proposed motion offsets can be expressed in the formulation of blur kernels. Specifically, in the general blur kernel model, a blurry image B is represented as $B = k * L + noise$, where k represents a blur kernel. In such a framework, our motion offsets can be regarded as an equivalent blur kernel $k(p_0, t_n)$ of the location p_0 over time $\{t_n\}_{n=0}^{N-1}$,

$$k(p_0, t_n) = \begin{cases} \frac{\delta(p - (p_0 + \Delta p_0^{t_n}))}{N}, & \text{if } p_0 + \Delta p_0^{t_n} \in L_s \\ 0, & \text{otherwise} \end{cases} \quad (5)$$

where $\delta(\cdot)$ denotes the Dirac delta function.

¹For most dynamic blur datasets, the middle instant frame is regarded as a sharp ground truth.

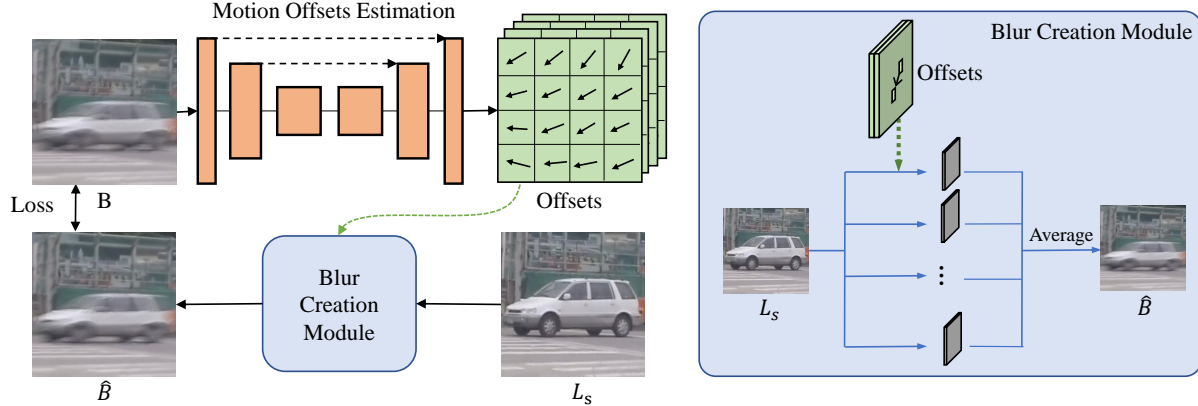


Figure 1: **Illustration of our proposed motion offset estimation method.** The figure on the left is our self-supervised motion offset generation network. It takes blurry images as input and outputs the corresponding motion offsets. Afterwards, the *blur creation module* (on the right) takes a sharp image and the extracted motion offsets to reconstruct the input blurry image.

Analyzing the equivalent formulation, the following differences between conventional blur kernels and our proposed motion offsets may exist. First, a time variable t_n is introduced as a new and important element to model the exposure process. Under reasonable assumptions (discussed in Section 4), our time-dependent motion offsets can act as a visualizable and explainable representation of dynamic motion. Since temporal information is considered, the learned motion offsets are capable of exploring pixel-wise exposure trajectories reflecting the changing velocity. Second, different from the weight matrix in a conventional blur kernel, as shown in Eq. (3), our motion offsets calculate a uniform average of wrapped frames over a time sequence. We assume each time step is equally discretized; thus, the degree of motion (or blur) in each position is represented by the learned spatial displacements $\{\Delta p^{t_n}\}$. Since the values of Δp^{t_n} are continuous, bilinear interpolation (Eq. (4)) is performed to derive the value on each discrete pixel position. Note that the bilinear interpolation operation plays the same role as the weight matrix in blur kernels. Third, benefiting from the spatial shift operation (*i.e.*, Δp^{t_n}), our equivalent blur kernel (*i.e.*, motion offset) will not be limited by size, shape, pattern, or resolution, as traditional kernels are. For example, compared to the dense blur kernels estimated in [4], where each kernel size is 33×33 , the proposed motion offsets only carry $N \times 2$ parameters². Finally, since our motion offsets, *i.e.*, the spatial displacements $\{\Delta p^{t_n}\}$, are compact and differentiable, the blur creation module can easily be integrated into deep neural networks and trained in an end-to-end manner.

4 Self-supervised Exposure Trajectory Recovery

As discussed in Section 3, based on the motion exposure mechanism, the proposed motion offset could replace conventional blur kernels. Exploiting its compact and differentiable advantages, we devise a self-supervised deep training scheme that performs motion offset estimation without any ground truths of the motion information. Moreover, considering the severely ill-posed nature of motion estimation from a single blurry image, we argue that the learned constraint-free motion offsets may not semantically match real-world motions. Then, we propose different trajectory constraints to form different pattern exposure trajectories.

²As shown our experiments, setting N as 15 already achieves extraordinary performance.

4.1 Self-supervised Motion Offset Estimation

The most difficult aspect of learning-based blur kernel estimation is the almost universal absence of ground truth blur kernels for real-world data. Thus, [11, 41] must use synthetic data for training. Due to our *blur creation module* being differentiable, we connect it with the motion offset estimation network to form a cyclical pipeline. Given a ground truth blurry image B and a sharp reference frame L_s , the motion offset estimation network takes B as an input and outputs N motion offsets; then, the *blur creation module* takes L_s and the motion offsets as input to reproduce the estimated blurry image \hat{B} . Fig. 1 illustrates this procedure. The motion offset estimation network is based on an encoder-decoder network with skip connections, and the detailed model structure is provided in Section 6.1.

The loss of this cyclic reconstruction can be written as:

$$\mathcal{L}_{circle} = \mathcal{L}_{l_2} + \lambda_{SSIM} \mathcal{L}_{SSIM}, \quad (6)$$

where \mathcal{L}_{l_2} and \mathcal{L}_{SSIM} denote the ℓ_2 loss and **SSIM** loss respectively. Both are applied to measure the difference between B and \hat{B} . We elaborate these two terms as follows:

$$\mathcal{L}_2 = \|B - \hat{B}\|_2^2, \quad (7)$$

$$\mathcal{L}_{SSIM}(P) = 1 - \mathbf{MS-SSIM}(\tilde{p}), \quad (8)$$

where \tilde{p} is the center pixel of patch P , and **MS-SSIM** denotes the multi-scale SSIM. A more specific definition and implementation can be found in [53]. The reason that we use the SSIM loss is that the ℓ_2 loss only weakly penalizes our output because it tends to generate average results, and the blurry image is already averaged. In this case, the SSIM loss more accurately measures the distance between two blurry images.

We also introduce other losses to regularize motion offsets. First, we apply a regularization loss to encourage offsets that search for nearby pixels as solutions. This benefits the situation in which there is a large smooth region, *e.g.*, the sky or ground, where large displacements (offsets) should be suppressed. Moreover, due to dynamic blur usually being continuous along the space, we apply the total variation loss to encourage spatial smoothness within offset maps. These two losses can be formulated as:

$$\mathcal{L}_{reg} = \frac{1}{Nwh} \sum_{n=1}^N \sum_{i=1}^w \sum_{j=1}^h M_n(i, j)^2, \quad (9)$$

$$\mathcal{L}_{tv} = \frac{1}{N} \sum_{n=1}^N \left(\frac{1}{(w-1)h} \sum_{i=0}^{w-1} |M_n(i, j) - M_n(i+1, j)| + \frac{1}{w(h-1)} \sum_{j=0}^{h-1} |M_n(i, j) - M_n(i, j+1)| \right), \quad (10)$$

where $M_n(i, j)$ denotes the location (i, j) in the n^{th} offset map.

In summary, the final loss function is a weighted sum of the above losses:

$$\mathcal{L} = \mathcal{L}_{circle} + \lambda_{reg} \mathcal{L}_{reg} + \lambda_{tv} \mathcal{L}_{tv}. \quad (11)$$

4.2 Different Constraints to Motion Offsets

If we directly learn all the motion offsets using the framework described above, namely a zero constraint (ZC) model, the results will be as shown in Fig. 2 (a). Though achieving impressive reblurring accuracy, its ill-posed nature creates the following problems: (1) the learned motion offsets are one of several possible solutions of blur formation, and since it is difficult to form them into an explicit trajectory as in real-world blur formation, the learned motion offsets are usually sub-optimal for describing realistic motion; and (2) although there exists the temporal variable t_n in our learned offsets, these offsets are disordered due to a lack of spatial-temporal relationship modeling.

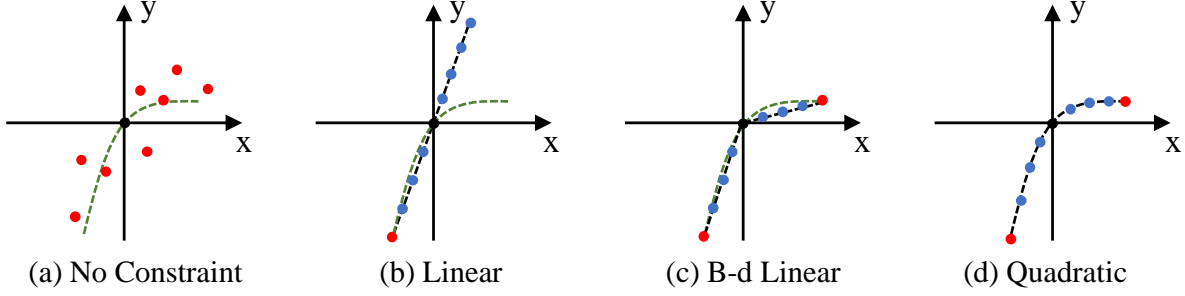


Figure 2: **Examples of motion offsets with different constraints.** Suppose the green curve is the ground truth exposure trajectory. (a)-(d) simulate the fitting results of motion offsets with no constraint, linear constraint, b-d linear constraint, and quadratic constraint, respectively. Red points are the offsets that output by the estimation network and blue points are calculated by the different constraints.

Therefore, we devise several constraints to reduce the ill-posed nature of motion estimation and to form the motion offsets into an explainable exposure trajectory.

(Bidirectional) linear trajectory constraint. The linear assumption is used to fit motion blur in many methods [14, 41, 11]. We also devise a linear trajectory constraint for motion offsets. Recall our assumption (Section 3) that the sharp image L_s represents the middle instant frame, *i.e.* $\Delta p^{t_{\text{mid}}} = (0, 0)$. To represent linear motion, the motion offset estimation network only needs to predict another point on the exposure trajectory. Suppose the blurred pixel is caused by uniform linear motion and the predicted offset Δp is an endpoint of the exposure trajectory, the other offsets can be derived as:

$$\Delta p^{t_n} = (1 - \frac{2n}{N-1})\Delta p, n = 0, \dots, N-1. \quad (12)$$

We attempt to predict the furthest point (endpoint) of the exposure trajectory based on the observation that the blurred edge is easier to capture and estimate.

Taking a further step, we can apply a bidirectional linear (b-d linear) constraint to our motion offsets. As shown in Fig. 2 (c), we predict two offsets $\Delta p_1, \Delta p_2$ to represent the start and end points of each exposure trajectory. Then, the other offsets can be calculated as:

$$\Delta p^{t_n} = \begin{cases} (1 - \frac{2n}{N-1})\Delta p_1, & n = 0, \dots, \frac{N-1}{2}, \\ (\frac{2n}{N-1} - 1)\Delta p_2, & n = \frac{N+1}{2}, \dots, N-1. \end{cases} \quad (13)$$

As shown in Fig. 2, this trajectory better fits a curve than the linear one.

Quadratic trajectory constraint. Although the bi-directional linear constraint already introduces a certain non-linearity into trajectory learning, the quadratic function can better approximate real-world motion [34, 49]. A quadratic curve can be derived when an object is moving with constant acceleration, a much stronger fitting than the (bi-)linear assumption. Thus, we devise a quadratic trajectory constraint to force a smooth quadratic trajectory on our motion offsets. Unlike previous works, which apply a quadratic trajectory between video frames, we extract this trajectory inside a single blurry frame. Specifically, we still predict two offsets $\Delta p_1, \Delta p_2$ as the start and end points of the exposure trajectory, with the other offsets written as:

$$\begin{aligned} \Delta p^{t_n} = & \frac{\Delta p_1 + \Delta p_2}{2} (\frac{2n}{N-1} - 1)^2 \\ & + \frac{\Delta p_2 - \Delta p_1}{2} (\frac{2n}{N-1} - 1), n = 0, \dots, N-1. \end{aligned} \quad (14)$$

Thus, motion offsets will be formed into a quadratic trajectory (Fig. 2 (d)). Note that since our motion offsets are modeled in equidistant time, the learned motion offsets not only match a curvilinear exposure

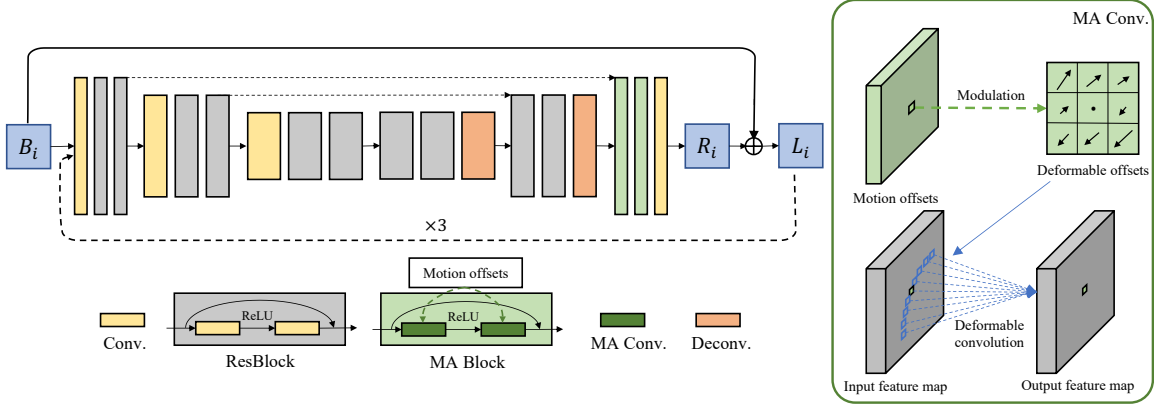


Figure 3: The proposed motion-aware deblurring network. An encoder-decoder residual architecture for image deblurring is shown on the left, while the schematic of a motion-aware convolution in the motion-aware block is shown on the right.

trajectory but also reflect the changing velocity. For example, a longer displacement between adjacent time steps corresponds to faster movement.

5 Applications Benefiting from Exposure Trajectory Recovery

5.1 Motion-aware Image Deblurring

To handle the challenging problem of dynamic scene deblurring, existing works employ complex network architectures to enlarge the model capacity, such as a multi-scale structure [23, 43, 9]. Some other methods [52, 30, 40] claim that spatially invariant convolution filters, *i.e.* spatially uniform and limited receptive fields are sub-optimal for modeling dynamic scene blur. With the learned exposure trajectories, we aim to design a spatial-variant deblurring network, which leads to a more compact and efficient model.

Infinite Impulse Response (IIR) Deconvolution. As derived in [52, 30], assuming that a blurry image and corresponding blur kernels are known, the latent sharp image can be formulated as:

$$L[x, y] = \frac{B[x, y]}{K[0, 0]} - \sum_{m, n=-M/2}^{M/2, M/2} \frac{K[m, n]B[x-m, y-n]}{K[0, 0]^2} + \frac{\sum_{m, n=-M/2}^{M/2, M/2} \sum_{i, j=-M/2}^{M/2, M/2} K[m, n]K[i, j]L[x-m-i, y-n-j]}{K[0, 0]^2}, \quad (15)$$

where L denotes a latent sharp image, B is a blurry image, and K represents blur kernels. $[x, y]$ denotes the pixel coordinates, and $M \times M$ is the size of the blur kernel. The last term in Eq. (15) can be infinitely expanded by replacing the term L with the weighted sum of K and B until it reaches the image boundary. According to this equation, [52, 30] drew two main suggestions: 1) the deblurring process requires a very large receptive field; and 2) for a CNN-based deblurring model, deconvolution filters should be directional/asymmetric. For example, if a blur kernel is linear and horizontal, according to Eq. (15), the latent pixels can be calculated using only horizontal blurry pixels, thus the deconvolution filters should also be pure horizontal. However, in most previous methods, it is difficult to establish the motion information (*i.e.*, kernel shape) from a blurry input. In this work, we propose a motion-aware deblurring network with spatial-variant convolution filters that are shaped by the learned exposure trajectories.

Motion-aware Deblurring Network. To build a spatial-variant convolution module, the deformable convolution unit [7] provides a general solution. In recent works [30, 40], spatial-variant deblurring modules based on deformable convolutions have achieved reasonable performance. However, since the ground truth of

the kernel shape is absent, these methods attempt to derive deformation offsets from encoded features of an input blurry image. We propose the motion-aware convolution (MA Conv.), which directly employs the learned motion offsets to model the aforementioned filter deformation. Our motion-aware convolution can be formulated as:

$$y(p_0) = \sum_{n=0}^N w(p_n) \cdot x(p_0 + \alpha \Delta p_0^{t_n}), \quad (16)$$

where x is an input feature map, y is an output feature map, and w is the weight of the deconvolution filter. For a 3×3 convolution filter, we will have $N = 8$, and $w(p_n)$ is the weight value of each location in a regular filter grid. Accordingly, we choose 9 motion offsets with $\Delta p_0^{t_n} = (0, 0)$ in the middle. Here, the original 3×3 filter is modulated as an exposure trajectory shaped filter, and the hyper-parameter α is used to control the scale of the modulation. In our experiments, we set the value of α as 0.1. In this way, the proposed motion-aware convolution takes full advantage of the information contained in motion offsets, *i.e.* both direction and magnitude, resulting in a more mathematically accurate deconvolution.

Here, we adopts the DMPHN(1-2-4) [51] as the backbone architecture of our motion-aware deblurring network, since it is relatively compact among the state-of-the-art models. As shown in Fig. 3, similar with the most existing image deblurring methods, the encoder-decoder structure is employed. Compare to the vanilla DMPHN(1-2-4), our motion-aware deblurring network can be easily derived by replacing the selected convolutional layers with the proposed motion-aware convolution. According to our experiments, adding the motion-aware convolutions in the last stage of the decoder achieved the best performance. In addition, to build a compact deblurring network, we do not employ the stack-DMPHN as Zhang *et al* [51]. Adding the motion-aware module can already achieve comparable results, and our model largely reduces the memory cost.

5.2 Warping-based Video Extraction from a Single Blurry Image

Different from conventional blur kernels, our motion offsets contain temporal information that could help us to restore time series from a blurry input. As indicated in Eq. (2), frame L^{t_n} can be obtained through a transformation $H(\cdot, \cdot)$. Now, with the deblurring result \hat{L}_s and the estimated motion offsets $\hat{\mathbf{P}}^{t_n}$, we can generate the estimated frame \hat{L}^{t_n} :

$$\hat{L}^{t_n} = \hat{L}_s(\mathbf{P} + \Delta \hat{\mathbf{P}}^{t_n}). \quad (17)$$

According to Sec 4.2, since we have added different trajectory constraints to motion offsets, theoretically we can interpolate arbitrary N offsets into our start and end offsets, which further leads to smooth or even slow-motion video output.

To our best knowledge, only two existing works have been capable of restoring a video sequence from a single blurry image. [16] first attempted to generated a video sequence from a single blurry image by training different networks to generate frames at different time t_n , only producing limited frames. [31] proposed a recurrent network to address temporal ambiguity, inferring the recurrent state at each time step t_n . Unlike these methods, we only need to calculate our motion offsets once, which is more time efficient. Moreover, these previous methods needed to collect a series of ground truth sharp frames for supervision, not only increasing the difficulty of data collection but also limiting the generated outputs to specific time intervals. Our motion offset estimation module is easy to train and requires fewer annotations. Moreover, during test, our model is more compact and efficient.

We demonstrate below two blurry image-related applications that may benefit from our exposure trajectory recovery. For deblurring, an increasing number of studies have shown that a deep learning black box may not ideally eliminate complex real-world blur and that the causes of blur should be explored to improve deblurring performance. Furthermore, the video extraction task can help us to interpret and visualize the exposure trajectories learned from a blurry image. We mainly focus on the definition and learning of the proposed motion offsets (and exposure trajectories), but in the future we hope to apply our exposure trajectory recovery to other related tasks.

Stage	Output	Layer Details
	$\frac{H}{2} \times \frac{W}{2}$	Space to Depth
Conv1	$\frac{H}{2} \times \frac{W}{2}$	$5 \times 5, 12, 16, \text{stride } 1$
ResBlock1	$\frac{H}{2} \times \frac{W}{2}$	$\begin{bmatrix} 5 \times 5, 16 \\ 5 \times 5, 16 \end{bmatrix} \times 3$
Conv2	$\frac{H}{4} \times \frac{W}{4}$	$5 \times 5, 16, 32, \text{stride } 2$
ResBlock2	$\frac{H}{4} \times \frac{W}{4}$	$\begin{bmatrix} 5 \times 5, 32 \\ 5 \times 5, 32 \end{bmatrix} \times 3$
Conv3	$\frac{H}{8} \times \frac{W}{8}$	$5 \times 5, 32, 64, \text{stride } 2$
ResBlock3	$\frac{H}{8} \times \frac{W}{8}$	$\begin{bmatrix} 5 \times 5, 64 \\ 5 \times 5, 64 \end{bmatrix} \times 3$
Bottleneck1	$\frac{H}{8} \times \frac{W}{8}$	$\begin{bmatrix} 1 \times 1, 64, 128 \\ 3 \times 3, 128, 64 \end{bmatrix}$
Dconv1	$\frac{H}{4} \times \frac{W}{4}$	$5 \times 5, 64, 32, \text{stride } 2$
Bottleneck2	$\frac{H}{4} \times \frac{W}{4}$	$\begin{bmatrix} 1 \times 1, 32 + 32, 128 \\ 3 \times 3, 128, 64 \end{bmatrix}$
Dconv2	$\frac{H}{2} \times \frac{W}{2}$	$5 \times 5, 64, 16, \text{stride } 2$
Bottleneck3	$\frac{H}{2} \times \frac{W}{2}$	$\begin{bmatrix} 1 \times 1, 16 + 16, 64 \\ 3 \times 3, 64, 32 \end{bmatrix}$
Dconv3	$H \times W$	$5 \times 5, 32, 32, \text{stride } 2$
Conv4	$H \times W$	$5 \times 5, 32, 4, \text{stride } 1$

Table 1: **Detailed architecture of the motion offset estimation network.** + denotes that a skip connection concatenates this layer with the corresponding layer in the encoder.

6 Experiments

In this section, we first introduce our training configuration before carrying out quantitative and qualitative comparisons between our method and state-of-the-art methods for motion estimation, image deblurring, and video extraction.

6.1 Implementation Details

We provide layer-wise details of our motion offset estimation networks in Table 1. H and W represent the height and width of an input blurry image. For training both the *motion estimation network* and *deblurring network*, we use Adam [18] for optimization, with $\beta_1 = 0.9$, $\beta_2 = 0.999$ and $\epsilon = 10^{-8}$. The learning rate is set initially to 10^{-4} and it is linearly decayed to 0. For motion offset estimation, we set the offset number to $N = 15$, $\lambda_{SSIM} = 0.1$, $\lambda_{reg} = 0.00002$, $\lambda_{tv} = 0.0005$. The number of training epochs varies for different datasets. According to our experiments, 800 epochs are sufficient to converge the *motion estimation network*, and 4000 epochs are sufficient to train the *deblurring network*. All weights are initialized using Xavier [10], and bias is initialized to 0.

6.2 Datasets

We employ two different datasets. The synthetic dataset provides ground truth blur kernels, while the GoPro dataset is synthesized from real-world frame with more challenging dynamic blur without ground truth blur kernels.

Synthetic Dataset. We follow the same approach as in [11] to generate blurry/sharp image pairs with pre-defined blur kernels. Specifically, blur kernels are represented by a motion flow map filled with pixel-wise non-uniform motion vectors. Each vector can form a linear blur kernel. Same as [11], we use images from BSD500 [2], which consists of 200 training images and 100 test images, as sharp ground truths. We then generate 50 motion flow maps for each training image and 3 motion flow maps for the test images. Finally, the sharp images are convolved with the corresponding flow maps to generate blurry images.

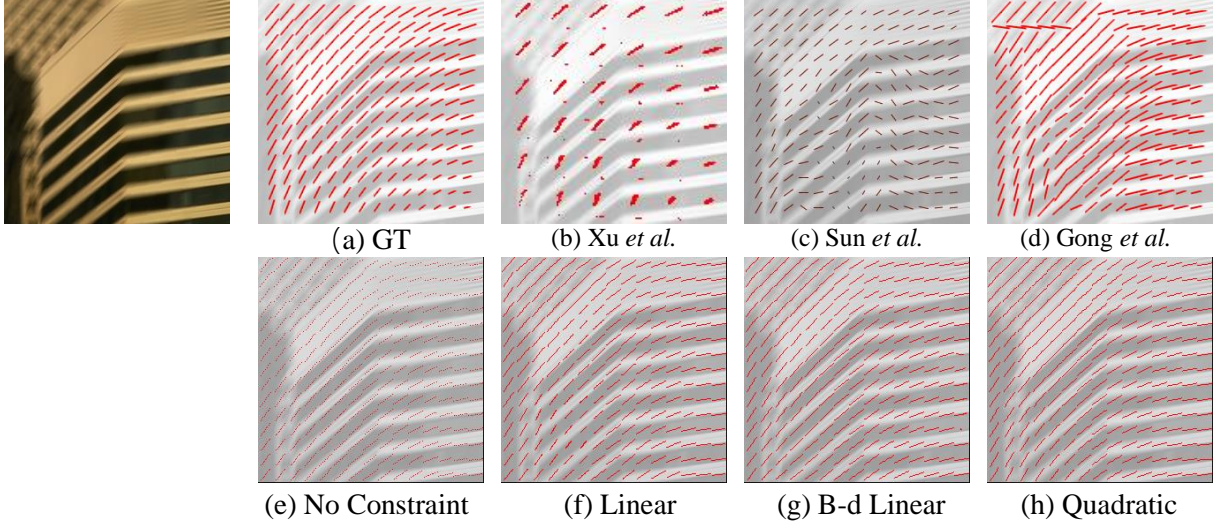


Figure 4: **Examples of motion estimation on the synthetic dataset.** The top row shows the blurry input, ground truth motion, and results of previous methods. The bottom row shows our estimated motion offsets under different constraints.

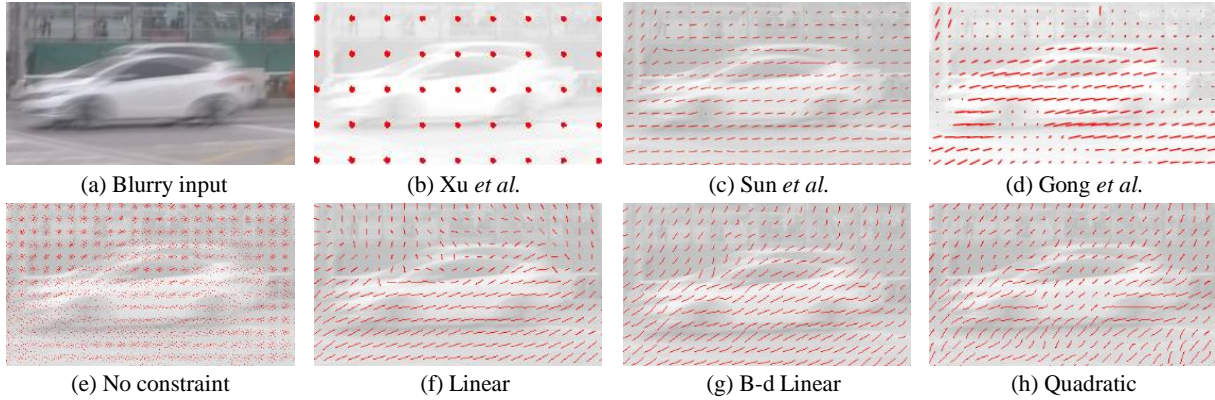


Figure 5: **Examples of motion estimation on the GoPro dataset.** The top row shows the blurry input and results of previous methods. The bottom row shows our estimated motion offsets under different constraints.

The **GoPro Dataset** [23] addresses the problem that synthetic data are different from real-world blurry images containing more complex dynamic motion. More realistic blurry images are generated by averaging consecutive short-exposure frames from a high frame rate video, *e.g.*, 240fps, taken from a GoPro camera. In this way, [23] collected 3214 blurry/sharp image pairs, and split them into a training set with 2103 pairs and a test set with 1111 pairs. In following experiments, unless stated, the quantitative results are based on the GoPro dataset.

6.3 Evaluation of Motion Offset Estimation

We compare the proposed exposure trajectory recovery with one conventional blur kernel estimation method (Xu *et al.* [48]) and two recent learning-based blur kernel estimation methods (Sun *et al.* [41] and Gong *et al.*

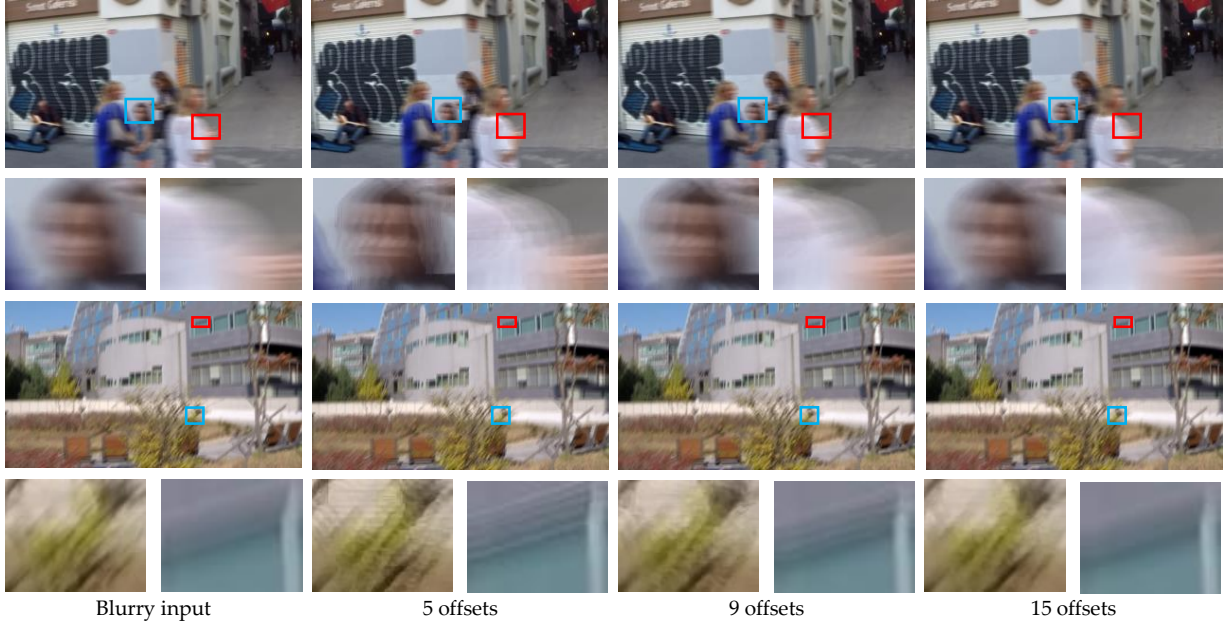


Figure 6: **The effect of offset number on blur creation.** Left to right show the ground truth blurry image, the result of the model with 5 offsets, the result of the model with 9 offsets, and the result of the model with 15 offsets. It is clear that increasing the number of offsets creates a smoother and more realistic blurry output.

	Model	Sun <i>et al.</i> [41]	Gong <i>et al.</i> [11]	ZC	Linear	B-d Linear	Quadratic
Synthetic	PSNR	29.34	37.61	37.62	37.34	38.64	38.9
	SSIM	0.9001	0.9818	0.9763	0.9857	0.9872	0.9882
	MSE	50.12	10.05	-	7.42	7.16	3.27
GoPro	PSNR	29.68	30.61	35.82	33.45	33.79	34.68
	SSIM	0.9282	0.9363	0.9800	0.9669	0.9687	0.9740
	Runtime(s)	45.2	8.4	0.011	0.011	0.011	0.011

Table 2: Quantitative comparison of motion estimation on both synthetic and the GoPro [23] dataset

[11]). Our comparisons are based on both the synthetic and GoPro datasets.

Evaluation Metrics. In order to evaluate the accuracy of motion estimation, we calculate the PSNR and SSIM metrics between the input blurry image and reblurred image via estimated blur kernel/motion offsets for both datasets. Specifically, the reblurred results of [41] and [11] can be obtained by convolving a sharp image with the estimated motion flow map. We also apply the MSE metric of motion to evaluate the synthetic data. This metric defines the mean squared error between the ground truth motion and estimated motion [11]. The MSE is easy to calculate in [41] and [11] since their estimated blur kernels share the same form as the ground truth, namely 2D vectors. However, our motion offsets are a set of points, so we calculate the vector of two endpoints as a simplification based on the assumption that the motion is linear. Note that we only provide the kernel visualization results of [48], since its blur kernel cannot be represented as a pixel-wise motion flow map like the others.

Motion Estimation on the Synthetic Dataset. Table 2 shows our quantitative comparisons on the synthetic dataset. Our quadratic model significantly outperforms the others according to all three metrics. Also, the other models with different constraints achieve comparable or better performance to [11]. It is noteworthy that [11] is learned in a supervised manner, thus demonstrating the effectiveness of our self-

# of motion offsets	5	9	15
PSNR	34.09	34.52	34.68
SSIM	0.9668	0.9727	0.974

Table 3: Comparison for the setting of offset numbers N .

	Proposed	w/o SSIM	w/o tv	w/o reg
PSNR	34.68	34.16	33.96	34.56
SSIM	0.974	0.97	0.9672	0.9727

Table 4: Ablation study for loss function.

supervised training scheme. Based on the two non-linear constraint models (our b-d linear and quadratic) producing results than the two linear constraint models ([11] and our linear), we infer that the non-linear constrain has a better fitting ability than the linear one.

We can also make some observations from Fig. 4. Xu *et al.* [48] generates non-trajectory kernels, for which we can only vaguely observe the flow after post-processing. Since Sun *et al.* [41] performs a patch-level prediction from a blurry input, it is usually misled by the smooth area. Gong *et al.* [11] shows more continuity across space, but there is also the possibility of when a region of predictions going wrong. Conversely, our motion offsets are more accurate and can perfectly fit into linear motion regardless of the employed constraints.

Motion Estimation on the GoPro Dataset. Since there is no motion ground truth for the GoPro dataset, the methods in [41, 11] cannot train their networks. Here, we employ their models pre-trained on the synthetic dataset and then test them on the GoPro test set. It may be unfair to directly compare these results with our own; however, to our best knowledge, no other method is trained without motion ground truths, so their results seem to be a legitimate reference.

Table 2 shows that the performance of [41, 11] decreases significantly with more complex dynamic scenes. This decrease in quality can also be observed in the example in Fig. 5. Xu *et al.* [48] fails to estimate large dynamic blur, and Sun *et al.* [41] is obviously inaccurate and tends to generate spatially uniform kernels. The results using Gong *et al.* [11], although spatially variant, tend to produce many non-blurry regions. Our results, however, show a different flow direction in the background and foreground, *e.g.*, the moving car. Further analyzing our different constraints, the non-linear constraints are better than the linear ones. Although the model with zero constraint achieved the best PSNR, it may because such a learning process does not consider recovering the exposure temporal ordering. The learned model is difficult to explore the semantic and explainable meaning of motion from the zero constraint results.

Ablation Studies. First, we discuss the setting of offset numbers N . As shown in Table 3, the model with $N = 15$ is notably better than the other models. The visual differences produced by altering the offset numbers are shown in Fig. 6. There is ghosting artifact with the model with 5 offsets, which becomes smoother as the offset number increases from 5 to 15. With 15 offsets, the result is very close to the ground truth blurry image. Since increasing the number of offsets has little effect on performance, we set $N = 15$, considering the balance between performance and efficiency.

To demonstrate the effectiveness of the proposed loss function, we trained a model with all the proposed losses (Model **Proposed**), one without the SSIM loss (Model **w/o SSIM**), one without the total variation loss (Model **w/o tv**), and one without the regulation loss (Model **w/o reg**). The quantitative results are shown in Table 4. The proposed loss combination is better than those without certain losses. Furthermore, the SSIM loss and total variance loss significantly improve motion estimation performance. Although the regulation loss has little influence on the metrics, it prevents the network from estimating large motion offsets in the smooth area.

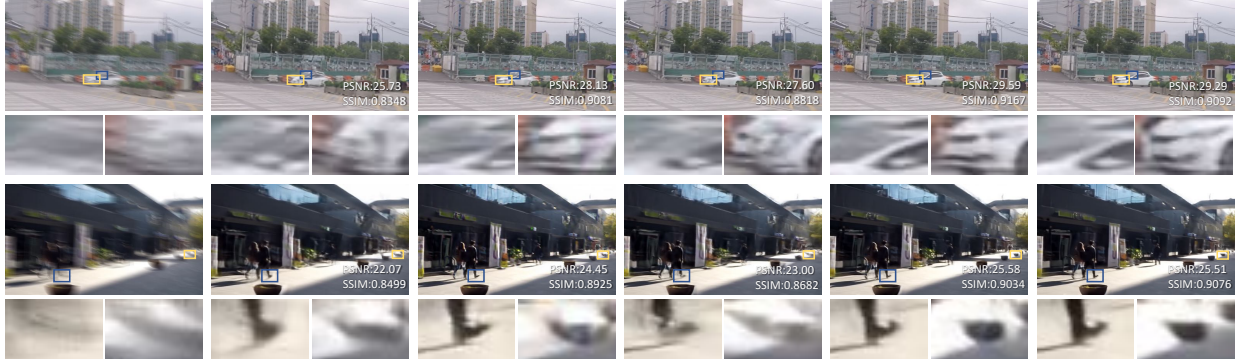


Figure 7: **Visual comparison with GoPro dataset.** From left to right, we show input, deblurring result of [43], [9], DMPHN [51], ours, and stack(4)-DMPHN [51] (best view in high resolutions).

6.4 Evaluation of Dynamic Scene Deblurring

We quantitatively and qualitatively compare our method with recent state-of-the-art dynamic scene deblurring methods: Kupyn *et al.* [20] based their method on a conditional GAN to obtain a more realistic texture; Nah *et al.* [23], Tao *et al.* [43], and Gao *et al.* [9] built multi-scale networks but with different parameter sharing and parameter independence schemes; Zhang *et al.* [51] applies a stacked Deep Multi-Patch Hierarchical Network (DMPHN), which is also the backbone network of our method. We also provide the deblurring results with [11] as representative of conventional MAP optimization. The quantitative results are presented in Table 5.

As illustrated in Table 5, our motion-aware deblurring network achieved comparable results to current state-of-the-art methods with respect to PSNR and achieved slightly better result with respect to SSIM. Note that, our model achieved such performance using a single-stack, which only costs about 30% of the model size compared to the model of the stack(4)-DMPHN. Considering the only difference between our model with DMPHN is the proposed motion-aware convolutional layer, it contributes 0.84 and 0.014 increasing in PSNR and SSIM, respectively. Also, as shown in Fig. 7, the visual results of ours are almost the same as stack(4)-DMPHN, while better than the other methods.

Besides verifying that the learned exposure trajectories could contribute to dynamic scene deblurring, we also conducted ablation studies to discuss the effects of different kinds of exposure trajectories. As Table 6 shows, compared to the baseline model (DMPHN), all kinds of exposure trajectories could improve the deblurring performance. Moreover, the Model Linear and the Model B-d linear perform slightly inferior to the Model Quadratic, owing to the less accurate of the motion estimation. Note that, though the exposure trajectories learned with zero-constraint (ZC) achieved the best score in above reblurring experiments (Table 2-GoPro), it demonstrated less effect in our deblurring module. A reasonable explanation is that the no-constraint motion offsets are only one of the ill-posed solutions for reblurring reconstruction, yet it will not be the most accurate trajectory estimation.

Model	Gong [11]	Nah [23]	Tao [43]	Kupyn [20]	Gao [9]	DMPHN[51]	Ours (Quadratic)	Stack(4)- DMPHN [51]
PSNR	26.89	29.08	30.26	29.55	30.92	30.21	<u>31.05</u>	31.20
SSIM	0.8639	0.9135	0.9342	0.9340	0.9421	0.9345	0.9485	<u>0.9453</u>
Size(MB)	54.1	303.6	33.6	35.4	46.5	21.7	<u>26.3</u>	86.8

Table 5: Quantitative deblurring results on GoPro dataset

Model	DMPHN [51]	Zero constraint (ZC)	Linear	B-d Linear	Quadratic
PSNR	30.21	30.79	30.82	31.04	31.05
SSIM	0.9345	0.9459	0.9462	0.9483	0.9485

Table 6: Ablation study of the different exposure trajectory in deblurring.



Figure 8: Comparison of video extraction results. In the top-down order, we show ours, result of [31], result of [16].

6.5 Evaluation of Video Extraction

To evaluate the performance of our approach for video extraction, we compare our results with those of Jin *et al.* [16] and Purohit *et al.* [31]. Since [16] is limited to small motion, we can see from Fig. 8 that the deblurring result (frame 4) and video extraction results (frames 1 and 7) of [16] both degrade significantly when handling large blur. The results of [31] and our own show relatively sharp frames and clear object movements. However, training [31] requires all the underlying blurry inputs frames. The main advantage of our method is that we can provide a quadratic trajectory. As shown in Fig. 9, we visualize the trajectory using feature point tracking [37]. Our quadratic motion offsets better fit the curve to the ground truth, especially in the second example. Finally, both [31] and our model can generate arbitrary numbers of frames, while [16] can only achieve a fixed number. The difference is that [31] generates the next frame in a recurrent network but we only need to interpolate in our trajectory after a single forward prediction. As a result, our network is more compact and faster. The runtimes of [16], [31], and our model are 1.1 s, 0.39 s, and 0.22 s respectively. We also provide an example of video extraction from real images in Fig. 10, demonstrating a good generalization ability of our proposed method. More video results can be found in our supplementary video.

7 Conclusion

Here we propose a self-supervised exposure trajectory recovery scheme to generate motion offsets which are superior to conventional blur kernels in many respects. By imposing different constraints, these offsets can fit into different exposure trajectories. Moreover, we utilize the learned motion offsets for image deblurring and video extraction from a single blurry image. Experiments show that our motion offsets can produce useful information for solving these tasks. However, the learned exposure trajectories are still limited to motion of constant acceleration, and may not perfectly fit real situations. We now aim to provide more accurate motion estimation and further improve the deblurring and video extraction tasks.

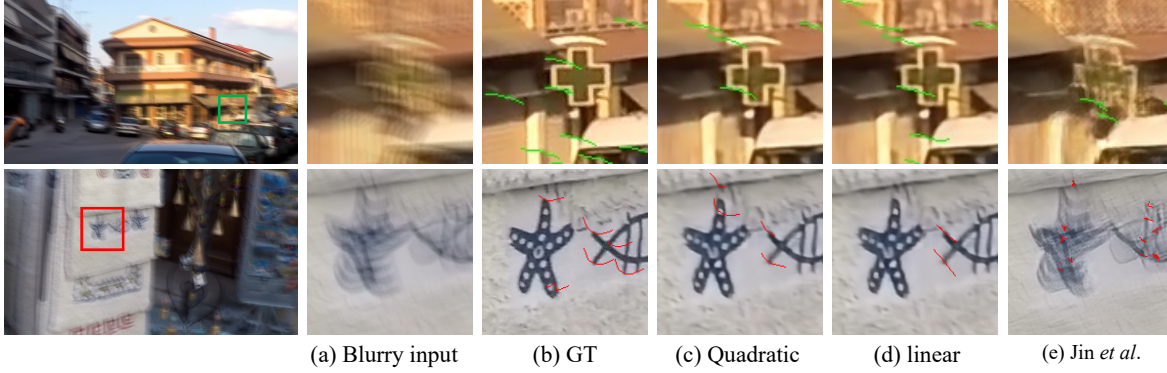


Figure 9: Visualized trajectory result of extracted frames (best view in high resolutions).

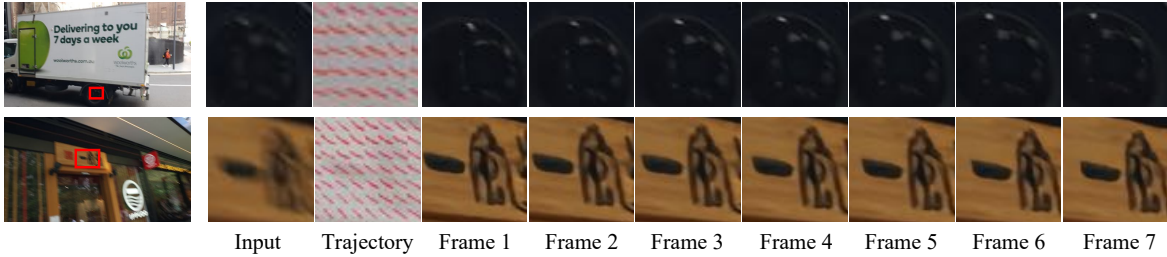


Figure 10: Video extraction results with real images.

References

- [1] I. Aizenberg, D. Paliy, C. Moraga, and J. Astola. Blur identification using neural network for image restoration. In *Computational Intelligence, Theory and Applications*, pages 441–455. Springer, 2006.
- [2] P. Arbelaez, M. Maire, C. Fowlkes, and J. Malik. Contour detection and hierarchical image segmentation. *IEEE transactions on pattern analysis and machine intelligence*, 33(5):898–916, 2010.
- [3] A. Chakrabarti. A neural approach to blind motion deblurring. In *European conference on computer vision*, pages 221–235. Springer, 2016.
- [4] H. Chen, J. Gu, O. Gallo, M.-Y. Liu, A. Veeraraghavan, and J. Kautz. Reblur2deblur: Deblurring videos via self-supervised learning. In *2018 IEEE International Conference on Computational Photography (ICCP)*, pages 1–9. IEEE, 2018.
- [5] L. Chen, F. Fang, T. Wang, and G. Zhang. Blind image deblurring with local maximum gradient prior. In *Proceedings of the IEEE Conference on Computer Vision and Pattern Recognition*, pages 1742–1750, 2019.
- [6] S. Cho and S. Lee. Fast motion deblurring. *ACM Transactions on graphics (TOG)*, 28(5):145, 2009.
- [7] J. Dai, H. Qi, Y. Xiong, Y. Li, G. Zhang, H. Hu, and Y. Wei. Deformable convolutional networks. In *Proceedings of the IEEE international conference on computer vision*, pages 764–773, 2017.
- [8] R. Fergus, B. Singh, A. Hertzmann, S. T. Roweis, and W. T. Freeman. Removing camera shake from a single photograph. In *ACM SIGGRAPH 2006 Papers*, pages 787–794. 2006.
- [9] H. Gao, X. Tao, X. Shen, and J. Jia. Dynamic scene deblurring with parameter selective sharing and nested skip connections. In *Proceedings of the IEEE Conference on Computer Vision and Pattern Recognition*, pages 3848–3856, 2019.

- [10] X. Glorot and Y. Bengio. Understanding the difficulty of training deep feedforward neural networks. In *Proceedings of the thirteenth international conference on artificial intelligence and statistics*, pages 249–256, 2010.
- [11] D. Gong, J. Yang, L. Liu, Y. Zhang, I. Reid, C. Shen, A. Van Den Hengel, and Q. Shi. From motion blur to motion flow: a deep learning solution for removing heterogeneous motion blur. In *Proceedings of the IEEE Conference on Computer Vision and Pattern Recognition*, pages 2319–2328, 2017.
- [12] A. Gupta, N. Joshi, C. L. Zitnick, M. Cohen, and B. Curless. Single image deblurring using motion density functions. In *European Conference on Computer Vision*, pages 171–184. Springer, 2010.
- [13] T. Hyun Kim, B. Ahn, and K. Mu Lee. Dynamic scene deblurring. In *Proceedings of the IEEE International Conference on Computer Vision*, pages 3160–3167, 2013.
- [14] T. Hyun Kim and K. Mu Lee. Segmentation-free dynamic scene deblurring. In *Proceedings of the IEEE Conference on Computer Vision and Pattern Recognition*, pages 2766–2773, 2014.
- [15] J. Jia. Single image motion deblurring using transparency. In *2007 IEEE Conference on Computer Vision and Pattern Recognition*, pages 1–8. IEEE, 2007.
- [16] M. Jin, G. Meishvili, and P. Favaro. Learning to extract a video sequence from a single motion-blurred image. In *Proceedings of the IEEE Conference on Computer Vision and Pattern Recognition*, pages 6334–6342, 2018.
- [17] C. Khare and K. K. Nagwanshi. Image restoration in neural network domain using back propagation network approach. *Image*, 2(5), 2011.
- [18] D. P. Kingma and J. Ba. Adam: A method for stochastic optimization. *arXiv preprint arXiv:1412.6980*, 2014.
- [19] O. Kupyn, V. Budzan, M. Mykhailych, D. Mishkin, and J. Matas. Deblurgan: Blind motion deblurring using conditional adversarial networks. In *Proceedings of the IEEE Conference on Computer Vision and Pattern Recognition*, pages 8183–8192, 2018.
- [20] O. Kupyn, T. Martyniuk, J. Wu, and Z. Wang. Deblurgan-v2: Deblurring (orders-of-magnitude) faster and better. In *Proceedings of the IEEE International Conference on Computer Vision*, pages 8878–8887, 2019.
- [21] A. Levin, Y. Weiss, F. Durand, and W. T. Freeman. Efficient marginal likelihood optimization in blind deconvolution. In *CVPR 2011*, pages 2657–2664. IEEE, 2011.
- [22] P. Liu, J. Janai, M. Pollefeys, T. Sattler, and A. Geiger. Self-supervised linear motion deblurring. *IEEE Robotics and Automation Letters*, 5(2):2475–2482, 2020.
- [23] S. Nah, T. Hyun Kim, and K. Mu Lee. Deep multi-scale convolutional neural network for dynamic scene deblurring. In *Proceedings of the IEEE Conference on Computer Vision and Pattern Recognition*, pages 3883–3891, 2017.
- [24] S. Nah, S. Son, and K. M. Lee. Recurrent neural networks with intra-frame iterations for video deblurring. In *Proceedings of the IEEE Conference on Computer Vision and Pattern Recognition*, pages 8102–8111, 2019.
- [25] S. K. Nayar and M. Ben-Ezra. Motion-based motion deblurring. *IEEE transactions on pattern analysis and machine intelligence*, 26(6):689–698, 2004.
- [26] J. Pan, Z. Hu, Z. Su, H.-Y. Lee, and M.-H. Yang. Soft-segmentation guided object motion deblurring. In *Proceedings of the IEEE Conference on Computer Vision and Pattern Recognition*, pages 459–468, 2016.

- [27] J. Pan, Z. Hu, Z. Su, and M.-H. Yang. l_0 -regularized intensity and gradient prior for deblurring text images and beyond. *IEEE transactions on pattern analysis and machine intelligence*, 39(2):342–355, 2016.
- [28] J. Pan, D. Sun, H. Pfister, and M.-H. Yang. Deblurring images via dark channel prior. *IEEE transactions on pattern analysis and machine intelligence*, 40(10):2315–2328, 2017.
- [29] L. Pan, R. Hartley, M. Liu, and Y. Dai. Phase-only image based kernel estimation for single image blind deblurring. In *Proceedings of the IEEE Conference on Computer Vision and Pattern Recognition*, pages 6034–6043, 2019.
- [30] K. Purohit and A. Rajagopalan. Region-adaptive dense network for efficient motion deblurring. In *AAAI*, pages 11882–11889, 2020.
- [31] K. Purohit, A. Shah, and A. Rajagopalan. Bringing alive blurred moments. In *Proceedings of the IEEE Conference on Computer Vision and Pattern Recognition*, pages 6830–6839, 2019.
- [32] J. Qiu, X. Wang, S. J. Maybank, and D. Tao. World from blur. In *Proceedings of the IEEE Conference on Computer Vision and Pattern Recognition*, pages 8493–8504, 2019.
- [33] S. Ramakrishnan, S. Pachori, A. Gangopadhyay, and S. Raman. Deep generative filter for motion deblurring. In *Proceedings of the IEEE International Conference on Computer Vision*, pages 2993–3000, 2017.
- [34] W. Ren, J. Pan, X. Cao, and M.-H. Yang. Video deblurring via semantic segmentation and pixel-wise non-linear kernel. In *Proceedings of the IEEE International Conference on Computer Vision*, pages 1077–1085, 2017.
- [35] C. J. Schuler, M. Hirsch, S. Harmeling, and B. Schölkopf. Learning to deblur. *IEEE transactions on pattern analysis and machine intelligence*, 38(7):1439–1451, 2015.
- [36] Q. Shan, J. Jia, and A. Agarwala. High-quality motion deblurring from a single image. *Acm transactions on graphics (tog)*, 27(3):1–10, 2008.
- [37] J. Shi et al. Good features to track. In *1994 Proceedings of IEEE conference on computer vision and pattern recognition*, pages 593–600. IEEE, 1994.
- [38] J. Shi, L. Xu, and J. Jia. Discriminative blur detection features. In *Proceedings of the IEEE Conference on Computer Vision and Pattern Recognition*, pages 2965–2972, 2014.
- [39] S. Su, M. Delbracio, J. Wang, G. Sapiro, W. Heidrich, and O. Wang. Deep video deblurring for hand-held cameras. In *Proceedings of the IEEE Conference on Computer Vision and Pattern Recognition*, pages 1279–1288, 2017.
- [40] M. Suin, K. Purohit, and A. Rajagopalan. Spatially-attentive patch-hierarchical network for adaptive motion deblurring. In *Proceedings of the IEEE/CVF Conference on Computer Vision and Pattern Recognition*, pages 3606–3615, 2020.
- [41] J. Sun, W. Cao, Z. Xu, and J. Ponce. Learning a convolutional neural network for non-uniform motion blur removal. In *Proceedings of the IEEE Conference on Computer Vision and Pattern Recognition*, pages 769–777, 2015.
- [42] Y.-W. Tai, P. Tan, and M. S. Brown. Richardson-lucy deblurring for scenes under a projective motion path. *IEEE Transactions on Pattern Analysis and Machine Intelligence*, 33(8):1603–1618, 2010.
- [43] X. Tao, H. Gao, X. Shen, J. Wang, and J. Jia. Scale-recurrent network for deep image deblurring. In *Proceedings of the IEEE Conference on Computer Vision and Pattern Recognition*, pages 8174–8182, 2018.

- [44] X. Wang, K. C. Chan, K. Yu, C. Dong, and C. Change Loy. Edvr: Video restoration with enhanced deformable convolutional networks. In *Proceedings of the IEEE Conference on Computer Vision and Pattern Recognition Workshops*, pages 0–0, 2019.
- [45] O. Whyte, J. Sivic, and A. Zisserman. Deblurring shaken and partially saturated images. *International journal of computer vision*, 110(2):185–201, 2014.
- [46] O. Whyte, J. Sivic, A. Zisserman, and J. Ponce. Non-uniform deblurring for shaken images. *International journal of computer vision*, 98(2):168–186, 2012.
- [47] L. Xu and J. Jia. Two-phase kernel estimation for robust motion deblurring. In *European conference on computer vision*, pages 157–170. Springer, 2010.
- [48] L. Xu, S. Zheng, and J. Jia. Unnatural l0 sparse representation for natural image deblurring. In *Proceedings of the IEEE conference on computer vision and pattern recognition*, pages 1107–1114, 2013.
- [49] X. Xu, L. Siyao, W. Sun, Q. Yin, and M.-H. Yang. Quadratic video interpolation. In *Advances in Neural Information Processing Systems*, pages 1645–1654, 2019.
- [50] Y. Yuan, W. Su, and D. Ma. Efficient dynamic scene deblurring using spatially variant deconvolution network with optical flow guided training. In *Proceedings of the IEEE/CVF Conference on Computer Vision and Pattern Recognition*, pages 3555–3564, 2020.
- [51] H. Zhang, Y. Dai, H. Li, and P. Koniusz. Deep stacked hierarchical multi-patch network for image deblurring. In *Proceedings of the IEEE Conference on Computer Vision and Pattern Recognition*, pages 5978–5986, 2019.
- [52] J. Zhang, J. Pan, J. Ren, Y. Song, L. Bao, R. W. Lau, and M.-H. Yang. Dynamic scene deblurring using spatially variant recurrent neural networks. In *Proceedings of the IEEE Conference on Computer Vision and Pattern Recognition*, pages 2521–2529, 2018.
- [53] H. Zhao, O. Gallo, I. Frosio, and J. Kautz. Loss functions for image restoration with neural networks. *IEEE Transactions on Computational Imaging*, 3(1):47–57, 2016.
- [54] S. Zheng, L. Xu, and J. Jia. Forward motion deblurring. In *Proceedings of the IEEE international conference on computer vision*, pages 1465–1472, 2013.